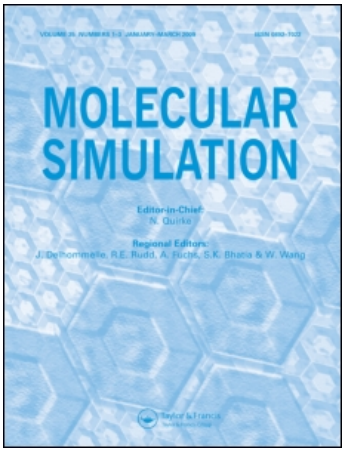

Molecular Simulation
Publication details, including instructions for authors and subscription information:
http://www.informaworld.com/smpp/title~content=t713644482

Hydration of ions under confinement

Ateeque Malani[a]; Sohail Murad[b]; K. G. Ayappa[a]
[a] Department of Chemical Engineering, Indian Institute of Science, Bangalore, Karnataka, India [b] Department of Chemical Engineering, University of Illinois, Chicago, IL, USA

Online publication date: 03 August 2010

To cite this Article Malani, Ateeque , Murad, Sohail and Ayappa, K. G.(2010) 'Hydration of ions under confinement', Molecular Simulation, 36: 7, 579 — 589
To link to this Article: DOI: 10.1080/08927021003752895
URL: http://dx.doi.org/10.1080/08927021003752895

Molecular Simulation
Vol. 36, Nos. 7–8, June–July 2010, 579–589

Taylor & Francis
Taylor & Francis Group

Hydration of ions under confinement

Ateeque Malani[a†], Sohail Murad[b] and K.G. Ayappa[a]*

[a]*Department of Chemical Engineering, Indian Institute of Science, Bangalore, Karnataka, India;* [b]*Department of Chemical Engineering, University of Illinois, Chicago, IL, USA*

(*Received 15 December 2009; final version received 5 March 2010*)

Molecular dynamics simulations are used to examine the changes in water density and hydration characteristics of NaCl solutions confined in slit-shaped graphitic pores. Using a structural signature, we define the hydration limit as the salt concentration at which a sharp drop in the hydration number is observed. At small pores ($H = 8.0–10$ Å), confined water does not possess bulk-like features and remains in a layered arrangement between two surfaces. Despite this high degree of confinement, ions are able to form a quasi-2D hydration shell between two surfaces. Our results indicate the strong propensity of ions to form the first hydration shell, even under extremely confined aqueous environments. The hydration of ions is seen to weakly perturb the oxygen density distributions between two surfaces. The hydration number of Na^+ reduces to about 4.15 at a pore width of $H = 0.8$ nm, when compared with the bulk hydration number of 6.25. At larger pore widths, above $H = 16$ Å, where bulk-like water densities are observed in the central regions of the pore, the hydration number is above 6.

Keywords: confinement ion-hydration; graphite; molecular dynamics

1. Introduction

The structure and dynamics of electrolyte solutions confined to nanopores are important in understanding processes such as transport in ion channels, ion solvation during hydration of proteins, ion exchange in zeolites and clays as well as the role of salts in proton exchange membranes. Many nanodevices being designed require manipulation of fluid flow in microchannels and nanochannels. The fluids often contain hydrated ions, and the effect of confinement on these hydrated ions can have a profound effect on the operation of these devices which include rapid sensors for bio- and chemical hazards/contaminants, nanorobots/nanomachines, lab-on-a-chip systems (nanoreactors) and nanotube clusters [1–4]. Although there is a wide body of literature on the structure and dynamics of electrolyte solutions [5–8], the effect of confinement has received less attention. Molecular dynamics simulations of sodium chloride solutions in carbon nanotubes reveal that ion-pairing is a strong function of the carbon nanotube radius [9]. At the smallest carbon nanotube of radius 0.65 nm, tightly bound ion pairs are formed at the axis of the nanotube. In addition to these studies which involve fully explicit representation of the water models, there have been some studies which employ a primitive model for the electrolyte [10,11]. In a preliminary molecular dynamics study, we examined the structural variations of sodium chloride solutions confined between graphite slit pores and contrasted the hydration levels with those observed in bulk solutions. In an 8 Å slit pore, we observed that the solubility reduces by a factor of 2 upon confinement [12].

Understanding the structure of confined aqueous solutions plays a central role in interpreting forces measured in the surface force experiment and swelling of clays. Experiments performed using the surface force apparatus indicate that water is able to form hydration layers when confined between mica surfaces and when ions are present in solution [13]. Additionally, the forces that are exerted by confined ionic solutions are influenced strongly by the presence of ions. The force–distance profile changes from having a single attractive minimum to an oscillatory nature as the ionic concentration is increased [13]. Molecular simulations of interstitial water in clays indicate that the ion hydration structure is mainly responsible for the observed swelling in clays [14,15]. In a recent study on water organisation in mica pores and on mica surfaces [16,17], it was observed that hydration of ions plays an important role in the structure as well as macroscopic properties of interfacial and confined water. Except for extreme confinement, the hydration structure around ions is not significantly perturbed at subnanometre confinement.

In this paper, we focus our attention on understanding the hydration properties of ions confined in graphitic slit-shaped pores. We carry out molecular dynamics simulations to investigate the hydration of ions for NaCl solutions confined between two graphite surfaces as a

*Corresponding author. Email: ayappa@chemeng.iisc.ernet.in
†Current address: Department of Chemical Engineering, University of Massachusetts, Amherst, MA, USA

ISSN 0892-7022 print/ISSN 1029-0435 online

DOI: 10.1080/08927021003752895
http://www.informaworld.com

function of both the spacing between two surfaces and the ionic strength. We examine the density distributions of water and ions as a function of the salt concentration, and comment on the structural variations as well as the hydration characteristics.

2. Simulation details

Figure 1 illustrates the schematic of the simulation box used to carry out molecular dynamics simulations of confined aqueous electrolyte solutions in a graphitic slit pore. The NaCl solution of varying concentrations is confined between two graphite surfaces of separation H. The pore width H is defined as the normal distance between the planes passing through the centres of the carbon atoms on opposing walls of the pore. The periodic boundary conditions are applied in x and y directions to construct an infinite pore in the lateral direction. The density of confined water as a function of pore widths was obtained from a previous grand canonical Monte Carlo simulation study of extended simple point charge (SPC/E [18]) water adsorption in graphitic slit pores [19]. The water loadings obtained from Liu and Monson [19] and the corresponding simulation box sizes used in this work are listed in Table 1. The reported changes in density with the concentration of aqueous NaCl solutions in bulk [20] were approximated to be valid under confinement as well, since no such data were available for confined fluids at similar concentrations. The density of NaCl solutions under confinement thus calculated was then used to estimate the number of molecules of water, Na^+ and Cl^- ions needed in an MD study for different concentrations and pore sizes (Table 2). A series of MD simulations in the *canonical (NVT) ensemble* were carried out at $T = 300$ K. The interaction between two atoms is modelled using 12-6 Lennard-Jones (LJ),

$$U_{ij}^{\mathrm{LJ}} = 4\varepsilon_{ij}\left[\left(\frac{\sigma_{ij}}{r_{ij}}\right)^{12} - \left(\frac{\sigma_{ij}}{r_{ij}}\right)^{6}\right] \tag{1}$$

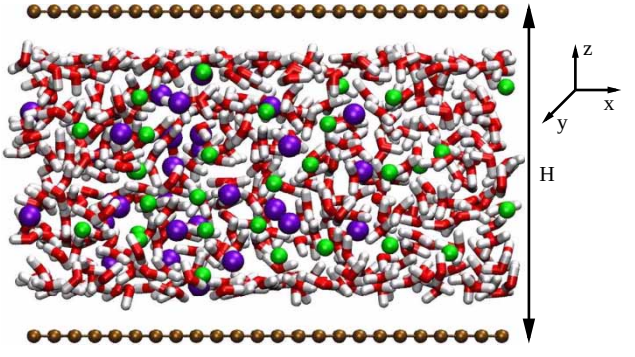

Figure 1. A snapshot of the simulated system illustrating the ionic solution confined between two graphite plates that make up a slit pore with width H. Brown, C; Red, O; White, H; Purple, Na^+; green, Cl^- (colour online).

Table 1. Pore loading (obtained from GCMC simulations [19]) and box size used in the molecular dynamics simulations.

Pore width (H) (Å)	ρ (Å^{-3})	L_x (Å)	L_y (Å)
20.0	0.02994	30.00	30.00
16.0	0.02836	30.00	30.00
10.0	0.02111	46.86	30.00
8.8	0.02048	55.38	30.00
8.0	0.01544	80.94	30.00

and Coulombic interactions

$$U_{ij}^{\mathrm{C}} = \frac{q_i q_j}{4\pi\epsilon_0 r_{ij}}, \tag{2}$$

where r_{ij} is the distance between two atoms i and j. The cross interaction terms (ε_{ij},σ_{ij}) in the LJ potentials are obtained using Lorentz–Berthelot mixing rules, $\varepsilon_{ij} = \sqrt{\varepsilon_{ii}\varepsilon_{jj}}$ and $\sigma_{ij} = (\sigma_{ii} + \sigma_{jj})/2$, where ε_{ii} and σ_{ii} are the interaction energy and molecular diameter of atom i, respectively. In Coulombic interactions, q_i is the charge on atom i and ϵ_0 is the vacuum permittivity. Water molecules are treated using the SPC/E model, Na^+ and Cl^- ions [21] are modelled using the primitive electrolyte models and interactions with the graphite carbons were obtained from an optimised model for graphite–water interactions [22]. The parameters for the interaction potentials are shown in Table 3. The geometry of water molecules are maintained using the RATTLE algorithm [23] for bond constraints. Both the LJ and Coulombic interactions were treated with a cylindrical cut-off (L_y/2). The system was simulated for 2.4 ns with a time step of 2 fs. During the initial 1.4 ns simulation time, the system was equilibrated and system properties were evaluated during the latter 1 ns. The simulations were performed in *canonical (NVT) ensemble* using a Gaussian thermostat [24,25].

3. Results

3.1 Ion hydration in bulk water

The structure of water around an ion, which can be obtained by X-ray diffraction and neutron-scattering experiments, was used to analyse the system [26–29]. We expect changes in the ion–water pair correlation function (PCF) as a function of concentration to be minimal in homogeneous solutions at low salt concentrations, since sufficient water molecules are available to completely hydrate the ions. Larger changes in the hydration shell and the ion–water PCF are expected to occur with an increase in the salt concentration. The disruption of the hydration shells would occur due to excess precipitated ions or ion pairs that are incompletely hydrated. The structural changes in hydration are expected to be reflected in the hydration numbers. Based on this, we define the hydration limit as the salt concentration, C_{hl},

Table 2. The number of water molecules (N_{water}) and ions ($N_{ions} = N_{Na^+} = N_{Cl^-}$) used in the simulations of bulk as well as confined aqueous electrolyte solutions.

Bulk aqueous electrolyte solution										
NaCl wt %	3	5	7	11	16	17	19	20	21	
N_{water}	296	294	292	287	281	279	276	275	273	
N_{ions}	3	5	7	11	16	18	20	21	22	
Confined aqueous electrolyte solution, $H = 20.0$ Å										
NaCl wt %	1	2	4	6	8	10	13	14	17	
N_{water}	536	534	530	527	523	518	512	509	502	
N_{ions}	2	3	7	10	14	18	24	26	32	
Confined aqueous electrolyte solution, $H = 16.0$ Å										
NaCl wt %	1	3	5	11	12	13	14	15		
N_{water}	406	403	401	391	389	388	386	384		
N_{ions}	1	4	6	15	16	18	19	21		
Confined aqueous electrolyte solution, $H = 10.0$ Å										
NaCl wt %	1	3	5	7	9	10	11	12	13	17
N_{water}	298	296	294	292	290	289	287	286	285	279
N_{ions}	1	3	5	7	9	10	11	12	13	18
Confined aqueous electrolyte solution, $H = 8.8$ Å										
NaCl wt %	1	3	5	6	9	10	11	12	14	16
N_{water}	298	296	294	293	290	289	287	286	283	281
N_{ions}	1	3	5	6	9	10	11	12	14	16
Confined aqueous electrolyte solution, $H = 8.0$ Å										
wt %	1	3	5	7	8	11	12	13		
N_{water}	298	296	294	292	291	287	286	285		
N_{ions}	1	3	5	7	8	11	12	13		

above which a sharp decrease in the hydration number of ions is observed. Although the hydration limit is expected to lie below the bulk solubility limit for the salt solution, it provides a suitable measure to compare the changes in hydration upon confinement. To verify such a hypothesis, and suitably examine the changes in the hydration limit under confinement, we first simulated bulk aqueous NaCl solutions at various concentrations. From the available density and concentration data [20], the number of molecules of salt and water at 300 K was obtained. To test the accuracy of our simulation scheme, the first peaks of the PCFs were compared with reported experimental and simulation results [30] (Table 4) for NaCl solutions in SPC/E water. The results in Table 4 indicate that the potentials used for studying the hydration of ions accurately capture the position of the first peak in the experimental ion–water PCF.

Our results show that as the concentration of salt increases within the complete solubility regime, the changes in the first peak of the ion–water PCF are quite small. This behaviour was consistently observed in all the ion–water PCFs examined as illustrated in Figure 2. A sharp change in the intensity of the first peak in the ion–water PCF occurred above a critical salt concentration. From the plot of the Cl^-—H PCF, we observe, for example, a 3.03% drop in the first peak with an increase in NaCl concentration from 7 to 16 wt% which, assuming

Table 3. Potential parameters for water, ions and carbon used in simulations.

Atoms	ϵ (kJ mol^{-1})	σ (Å)	q (e)
O[a]	0.6502	3.166	−0.8476
H[a]	0.0	0.0	+0.4238
Na^{+}[b]	0.48208	2.275	+1
Cl^{-}[b]	0.4184	4.409	−1
C[c]	0.29628	3.2145	0.0

[a] Berendsen et al. [18]. [b] Pal et al. [21]. [c] Werder et al. [22].

Table 4. Structural results for first solvation shell maxima.

		Simulations r (Å)	
PCF	Experiments[a,b,c,d] r (Å)	Literature[e]	This work
Cl^-—H	2.22–2.60	2.25	2.23
Cl^-—O	3.10–3.35	3.21	3.23
Na^+—H	–	2.90	2.89
Na^+—O	2.38–2.40	2.33	2.33

[a] Neilson and Enderby [26]. [b] Cummings et al. [27]. [c] Newsome et al. [28]. [d] Enderby and Neilson [29]. [e] Chandrasekhar et al. [30].

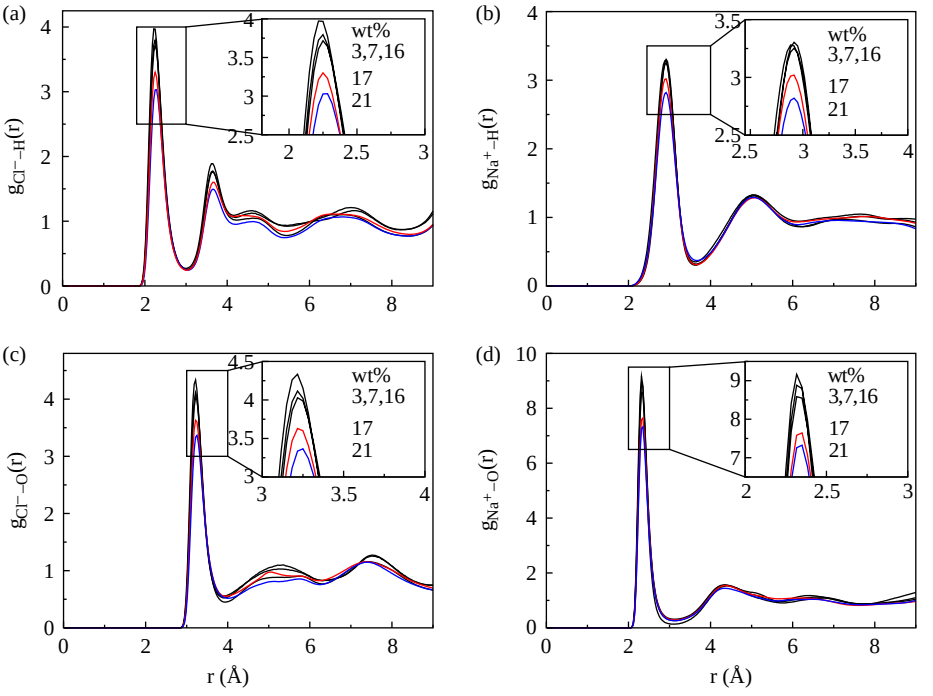

Figure 2. Ion–water PCFs for bulk electrolyte solutions. For clarity, only selected PCFs at various salt concentrations are shown. The sharp drop in the intensity of the first peak, as the salt concentration is increased, is evident from all the ion–water PCFs.

linearity, corresponds to a 0.33% drop per % change in concentration, whereas we see a sharp drop in the first maxima of 13.44% with an increase in concentration from 16 to 17 wt%. Thus, the ratio of the differential change, which is almost 40, clearly reflects a dramatic structural change occurring in the hydration shell of the Cl^- ion. We refer to this concentration at which the sharp change in the PCF is observed, as the hydration limit. Further increase in the concentration above the hydration limit leads to a drop in peak intensity of approximately 2.3% per % change in concentration. These relative changes in the intensity of the first peak in the PCF were observed for all the PCFs, as shown in Figure 2. In order to precisely define the hydration limit, we evaluated the hydration numbers, N_h, by integrating the Na^+—O PCF up to the first minima, which occurred at 2.33 Å. The variation in N_h as a function of the salt concentration is shown in Figure 3. The results show that the hydration numbers are essentially constant (within the simulation error bars) up to the hydration limit which occurs at an NaCl concentration corresponding to $C_{hl} = 16$ wt%. In simulations, the solubility limit of NaCl salt in water (SPC/E) is found to be 23 wt% [31]. This is slightly lower than the experimentally observed value of 25 wt% [20]. Beyond the hydration limit, there is a sudden drop in the hydration number. Examination of the configuration of ions in our simulations revealed a significant increase in the number of ion pairs (Na^+—Cl^-) in the solutions once the hydration limit is reached or exceeded. This leads to fewer water molecules surrounding each ion leading to the resultant drop in the peak of the PCF and hydration numbers. Figure 4(a) shows the snapshot of one of the Na^+ ions hydrated by water molecules at a low salt concentration of 1 wt%. At low concentrations, the hydration shell is complete and one can observe that the sodium ion is surrounded by six oxygen atoms that make up the first hydration shell (Figure 4(a)). At a higher salt concentration of 17 wt% above the hydration limit, the number of water molecules in the first

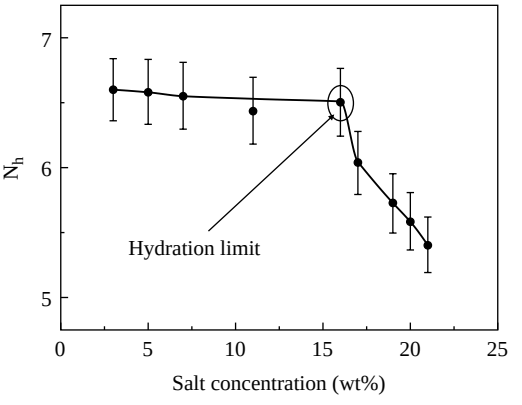

Figure 3. Variation in hydration number, N_h, as a function of salt concentration. N_h is obtained by integrating the Na^+—O PCF (Figure 2(d)) up to the first minima ($r = 2.33$ Å). The drop in the ion–water PCF (Figure 2) gives rise to a sharp decrease in N_h, which is used as criteria to define the concentration corresponding to the hydration limit C_{hl}.

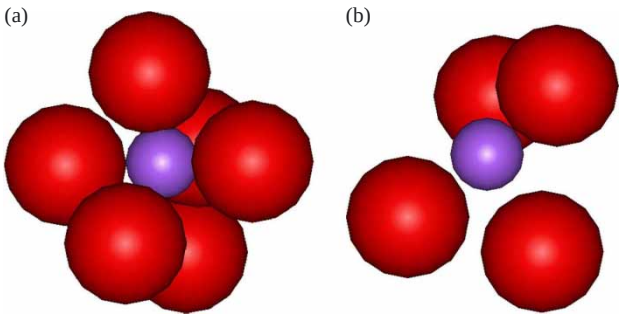

Figure 4. Snapshot illustrating the hydration structure of ions in bulk water: (a) dilute solution, 1 wt% salt concentration and (b) high salt concentration of 17 wt% above the, hydration limit. The snapshots illustrate the disruption in the hydration shells as the salt concentration is increased. Red, water oxygen; purple, sodium ion (colour online).

hydration shell drops and this effect is seen in the snapshot shown in Figure 4(b), where a fewer number of water molecules occupy the first hydration shell of the sodium ion. We would like to point out that the hydration number N_h obtained by integrating the first peak of the PCF is sensitive to the integration scheme. In our previous study [12], a simple trapezoidal integration on the raw data tended to underestimate the peak areas resulting in smaller values of N_h at lower salt concentrations. Here, we have used a cubic spline interpolant during integration and the N_h values are relatively constant up to the hydration limit, consistent with the trends observed for the PCFs.

3.2 *Ion hydration under confinement*

In this section, we examine the hydration characteristics of NaCl solutions confined in the graphite slit pore. Since all ion–water PCFs showed similar behaviour as the salt concentration was increased (i.e. significant drop in the first peak), we report only Na^+—O PCFs for pore sizes in the range $H = 8–20$ Å. The PCF calculated under confinement is based on the bulk definition. We first analyse the results for the smallest pore width of $H = 8$ Å. Figure 5 illustrates the layer density distribution for the water oxygen, Na^+ and Cl^- ions as a function of the salt concentration. The oxygen density distributions indicate that water is located within 1 Å of the central regions of the pore and a slight increase in density is observed in the regions adjacent to the graphite surface. Both the Na^+ and Cl^- ion densities indicate that the ions are located in the central regions of the pore for all the salt concentrations examined. Interestingly, the oxygen densities remain relatively unchanged as the salt concentration is increased. However, a small increase in the intensity of the peaks closer to the graphite surface is observed. The corresponding PCF for Na^+—O is illustrated in Figure 6(a) and the variation in the hydration number, N_h, as a function the salt concentration is illustrated in Figure 6(b). Similar to the

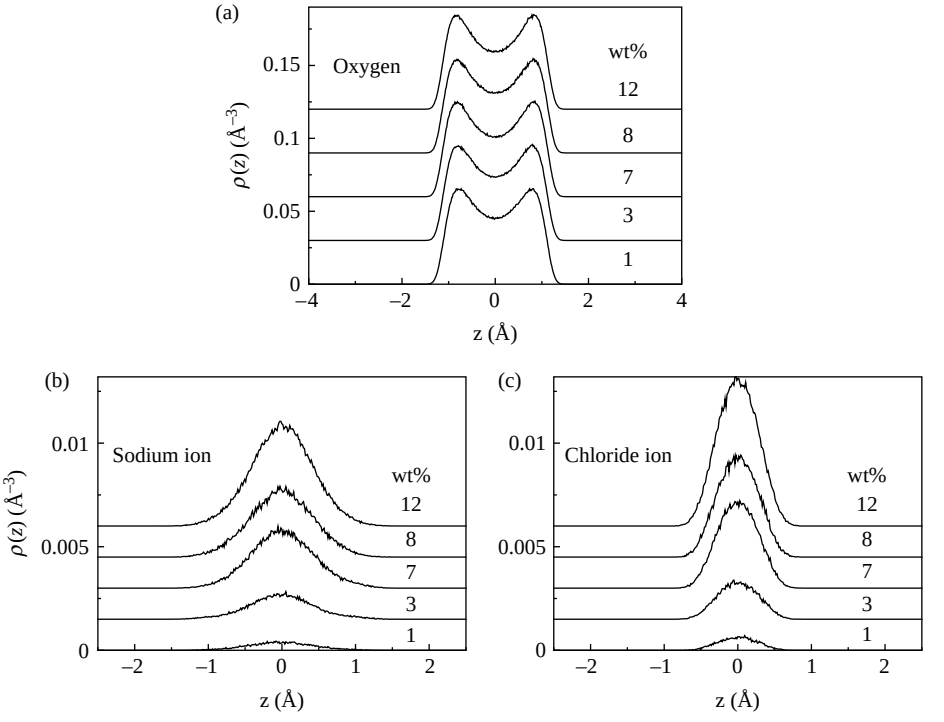

Figure 5. The density distribution of (a) water (oxygen), (b) Na^+ and (c) Cl^- ions between graphite surfaces of separation $H = 8$ Å. Water molecules as well as ions are aligned in the central regions of the pore.

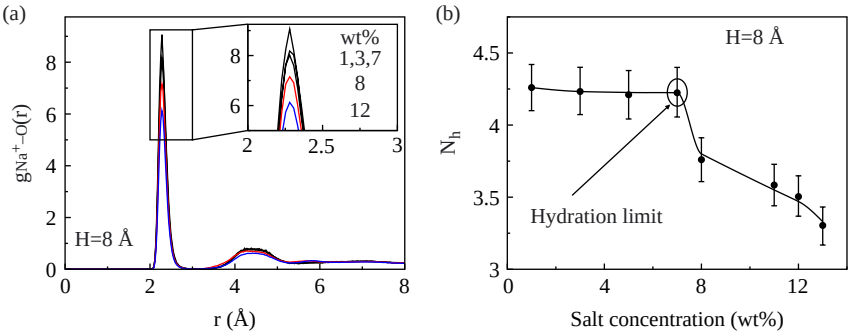

Figure 6. (a) Ion–water (Na^+—O) PCF, $g_{Na^+—O}$ (r), and corresponding (b) hydration number, N_h, variation as a function of salt concentration for $H = 8$ Å is illustrated. Also shown is the hydration limit $C_{hl} = 7$ wt% in (b).

trends observed in bulk water, an increase in the salt concentration results in a rapid decrease in intensity of the first peak of the PCF. From the N_h data, the hydration limit is seen to occur at 7 wt% NaCl. In contrast, the hydration limit for bulk water was observed at 16 wt%.

The quasi-2D nature of the confinement reduces the hydration number for Na^+ at the low salt concentration to a value of around 4. The corresponding value of N_h for bulk water was around 6. Despite the drop in hydration number, the positions of the peaks in the Na^+—O PCF (Figure 6(a)) occur at similar radial positions, as was observed for the bulk salt solutions (Figure 2(a)). Snapshots for the water and ion configurations for $H = 8$ Å situation are illustrated in Figure 7 for both low and high salt concentrations. At a low salt concentration of 1 wt%, the formation of solvation shells around both the Na^+ and Cl^- ions is clearly visible (Figure 7(a)). The quasi-2D solvation shell around the Na^+ ions distinctly reveals the presence of four water molecules in the first hydration shell with the oxygen atoms of the water molecules directed towards the Na^+ ion. At the hydration limit (7 wt%), the snapshot in Figure 7(b) illustrates the onset of ion-pairing under confinement and a configuration wherein the Cl^- ion is surrounded by three Na^+ ions is clearly observed.

The density distributions for water and ions for the larger pore widths, 10, 16 and 20 Å, are illustrated in Figures 8, 9 and 10, respectively. The density distribution of water (oxygen) compares very well with the structure reported by Striolo and co-workers [32] at similar pore densities. It was also observed that for pore widths $H \geq 16$ Å, the water (oxygen) density as well as the order parameter in the central regions of the pore assumes bulk values. We note that the density profiles for oxygens are

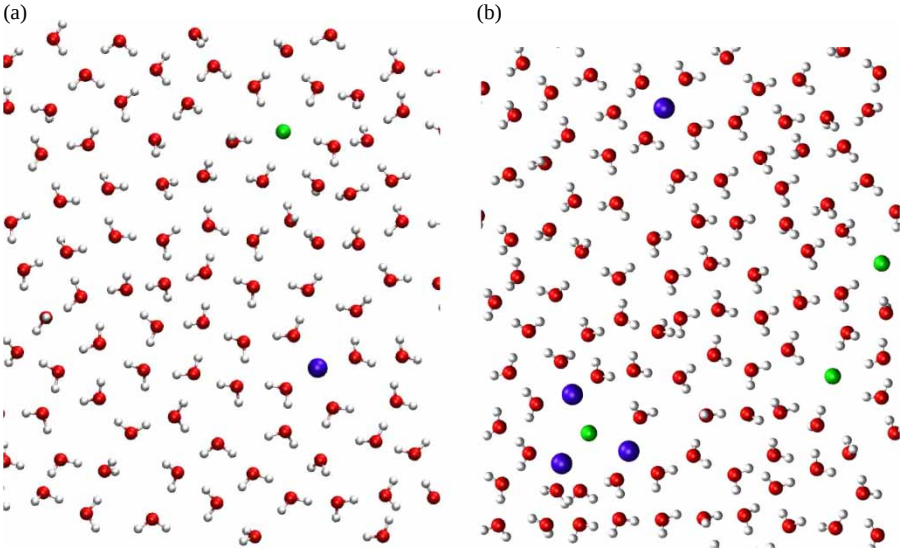

Figure 7. Snapshot illustrating the hydration structure of ions for the $H = 8$ Å graphite pore at (a) 1 and (b) 7 wt%. The quasi-2D solvation of ions is illustrated at the low salt concentrations and the formation of hydration shells for both the Na^+ and Cl^- ions is distinctly visible (a). The snapshot (b) illustrates the onset of ion-pairing where the Cl^- ion is surrounded by Na^+ ions. Red, water oxygen; purple, Na^+; green, Cl^-; white, water hydrogen (colour online).

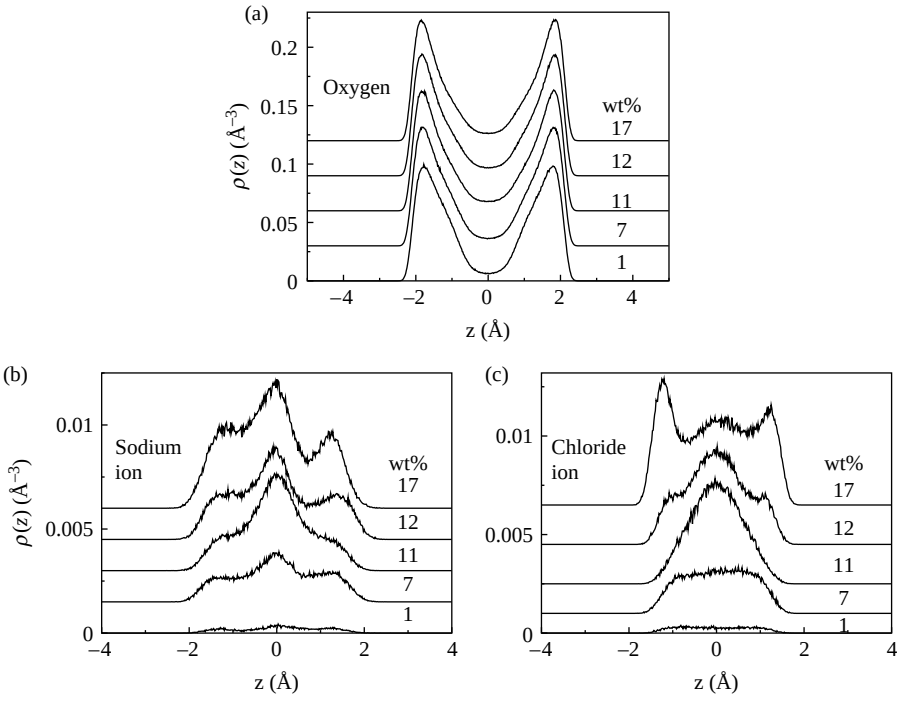

Figure 8. The density distribution of (a) water (oxygen), (b) Na^+ and (c) Cl^- ions between graphite surfaces of separation $H = 10$ Å. Here, water forms two distinct layers in the pore and at low concentrations, the ions are situated between the oxygen layers to enable effective hydration.

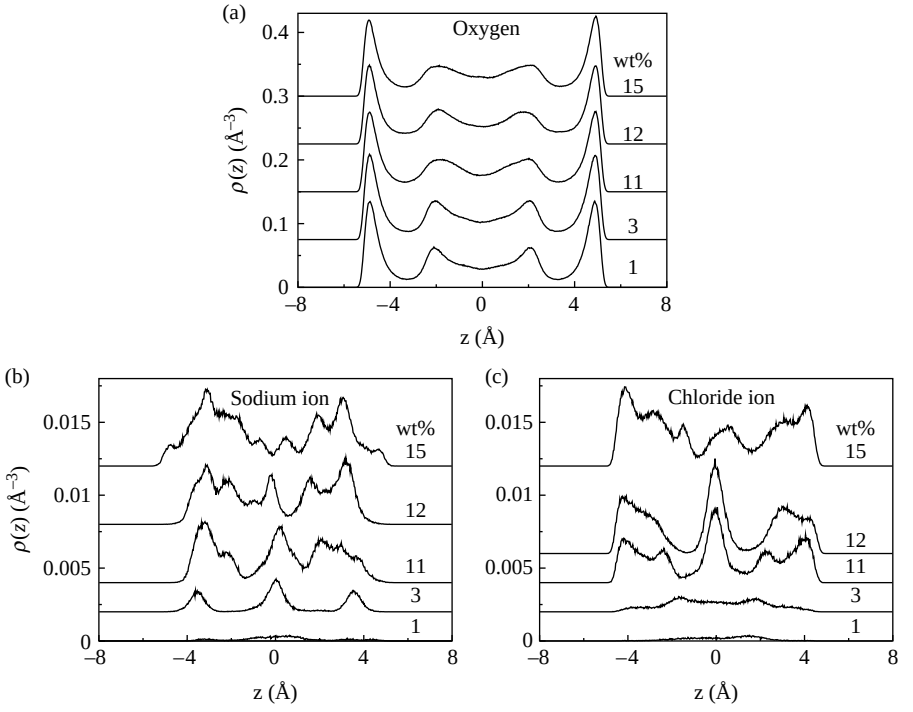

Figure 9. The density distribution of (a) water (oxygen), (b) Na^+ and (c) Cl^- ions between graphite surfaces of separation $H = 16$ Å. The ions occupy the position between the water layers to facilitate hydration without significantly disrupting the layering in the system.

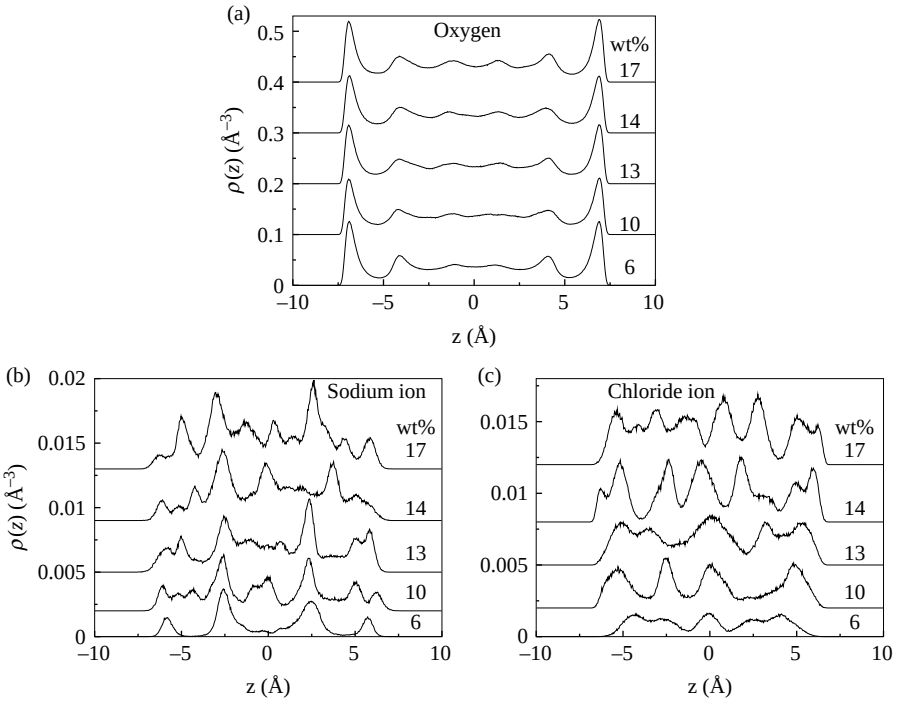

Figure 10. The density distribution of (a) water (oxygen), (b) Na^+ and (c) Cl^- ions between graphite surfaces of separation $H = 20$ Å. The ions occupy the position between water layers to facilitate the hydration without disrupting layering in the system.

symmetric and the density profiles for the ions are asymmetric particularly at the higher salt concentrations. This could be related to the insufficient sampling times for the ions themselves. At $H = 10$ Å, the oxygen density reveals the formation of two distinct layers within the pore and both the Na^+ and Cl^- ions occupy the central regions of the pore (Figure 8). At the largest pore width examined ($H = 20$ Å), water density in the central regions of the pore are bulk-like and a weak enhancement in the density oscillation is observed as the salt concentration is increased. Figure 11(a), (c), (e) and (g) illustrates the ion–water (Na^+O) PCF obtained for various salt concentrations in the pore of width $H = 8.8$, 10, 16 and 20 Å, respectively. We have shown only the Na^+—O PCFs in Figure 11. The hydration numbers obtained by integrating the Na^+—O PCF are shown in Figure 11(b), (d), (f) and (h), respectively, where the hydration limits have been indicated in the plots. Similar to the trends observed for the bulk electrolyte, the Cl^-—H PCFs also show a sharp reduction in the peak intensities at similar salt concentrations. The corresponding pair distribution functions have been shown in an earlier work [12]. We observe that aqueous electrolyte solutions under confinement also show similar limiting hydration behaviour and a hydration limit can clearly be identified from the hydration number data for all the pore widths examined. The transition from the fully hydrated situation to a partially hydration state is sharp and occurs over a salt concentration change of within 1 wt%. Although we have not investigated the onset of ion-pair formation in detail, some sample calculations and observation of particle snapshots indicate that the hydration limit is associated with the formation of ion pairs. An example of this situation was illustrated in Figure 7(b). The Na^+—Cl^- PCF computed for $H = 16$ Å revealed a strong first peak formation at concentrations corresponding to the hydration limit. Below the hydration limit, the PCF did not reveal the formation of ion pairs.

In addition to the hydration limit which indicates the onset of ion-pairing in these systems, it is also of interest to examine the hydration levels of ions before the hydration limit is reached and contrast this hydration regime under confinement where sufficient water exists in the pores to the hydration observed in the bulk at low salt concentrations. The hydration numbers for pores $H = 8$, 8.8, 10, 16 and 20 obtained from the plateau regions observed in the hydration number vs. salt concentration data indicate hydration numbers of 4.15, 5.25, 5.5, 6.0 and 6.1, respectively. The corresponding value observed for the bulk solution is 6.25. For pore widths above 16 Å, the hydration numbers are only slightly smaller than the number observed for bulk water, indicating that at lower salt concentrations there is sufficient water to complete the hydration shells of the confined ions. At $H = 20$ Å (Figure 10(a)), water in the central regions of the pore begin to acquire bulk-like features based on the reduced density oscillations and approach to bulk-water densities.

Despite the strongly layered configuration of water observed for pore widths below $H \leq 10$ Å (Figures 8(a)

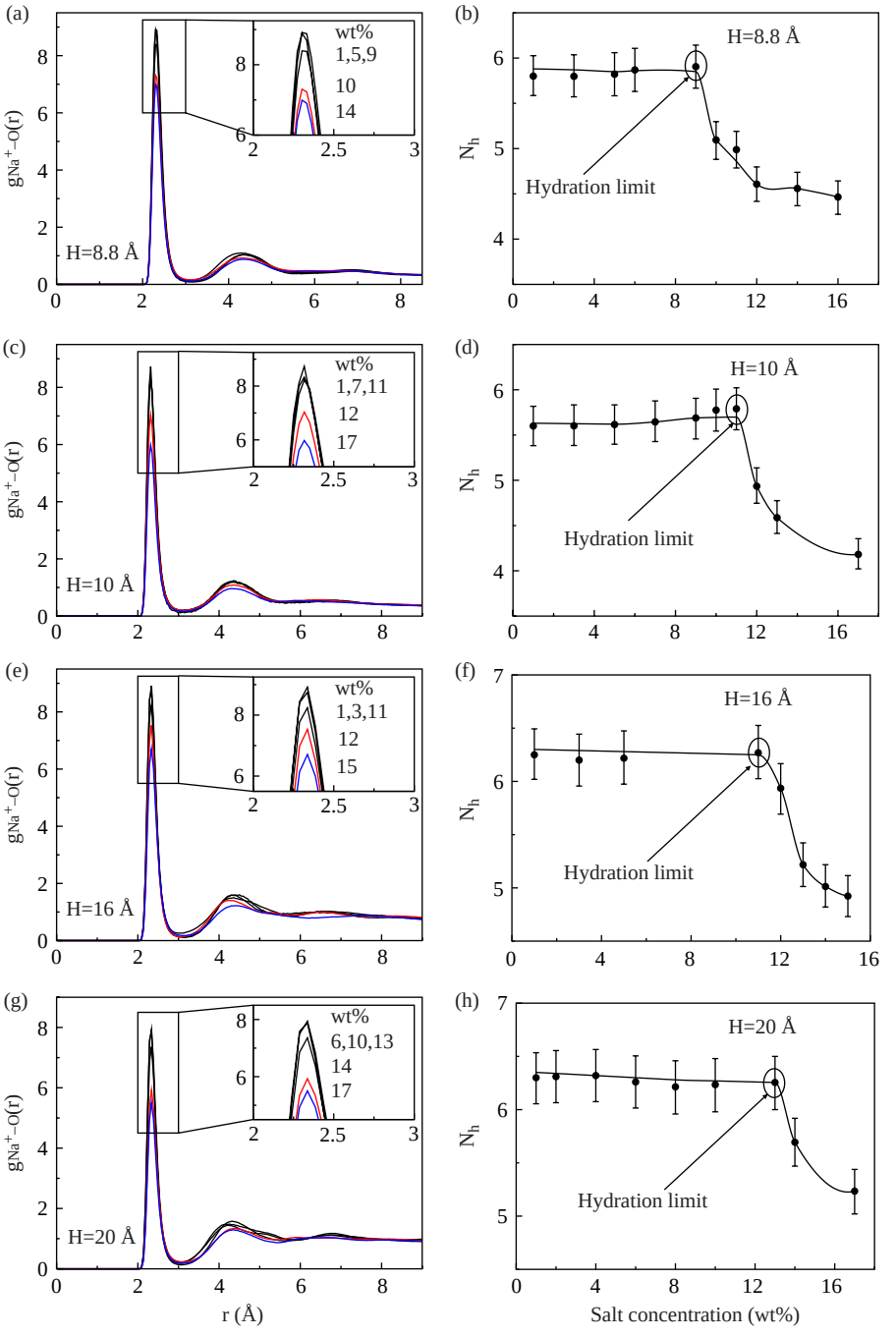

Figure 11. The ion–water (Na^+—O) PCF, $g_{Na^+-O}(r)$, of Cl^- ions obtained for pore width (a) $H = 8.8$, (c) 10, (e) 16 and (g) 20 Å and the corresponding hydration number, N_h, variation as a function of salt concentration.

and 5(a)), the drop in the low salt hydration number is not very sharp and remains above 5 for $H = 8.8$ Å. The propensity of the ions to maximise electrostatic interactions with water determines the location of the ions relative to water within the pore. At smaller pore widths ($H = 8.0$ and 8.8 Å), the ions are located along the central regions of the pore where the water density is the lowest, enabling the ions to form the first solvation shells without having to destroy the layered structure of water in the pore. This trend persists for the larger pores where both the Na^+ and Cl^- ions are situated between the oxygen layers that form in the pore. This relative positioning of ions in the pore aids in preserving the hydration shells and only at the smallest pore width of $H = 8$ Å does the hydration number drop to 4.15. These trends suggest that hydration under these extreme confinements is driven by the strong

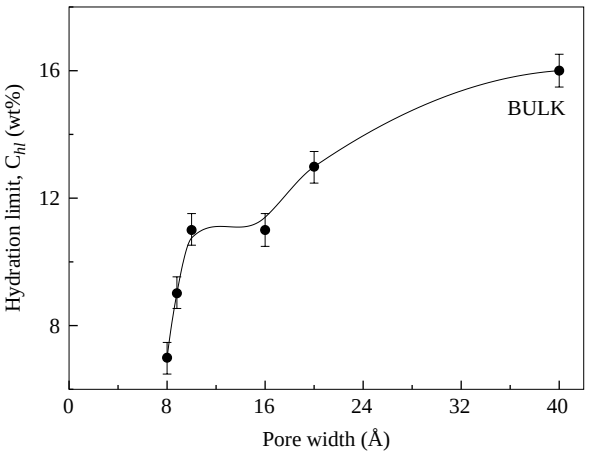

Figure 12. The effect of confinement on the hydration limit C_{hl} of ions. Due to strong confinement, the C_{hl} drops by around 55% of the bulk value for $H = 8$ Å. The sharp decrease in C_{hl} corresponds to water primarily being present as bound water in the pore (Figures 5(a) and 8(a)). Also shown is the bulk value of C_{hl} at $H = 40$ Å for reference only.

enthalpy of hydration when compared with the loss of entropy due to disruption of the water–water hydrogen bond network.

Figure 12 summarises the hydration limit, C_{hl}, for the various pore widths examined. The concentration at which the hydration limit, C_{hl}, is observed for bulk water is also indicated for reference. The most noticeable feature in the data is the sharp drop in the hydration limit as the pore width is reduced below 10 Å. At the smallest pore width ($H = 8$ Å) examined, the NaCl concentration at which the hydration limit occurs is reduced by about 55% of the bulk value and at $H = 10$ Å a reduction of about 30% is observed. From the various cases examined in this study, it is likely that a significantly larger pore width than 20 Å is required to recover the bulk C_{hl} of 16 wt%. Examination of the Cl^- and Na^+ ion distributions at $H = 20$ Å, where water in the central regions of the pore is bulk-like, reveals that the ions are strongly layered, indicating that this relative positioning of ions is required in order to keep them solvated in the confined region. We have not carried out simulations beyond $H = 20$ Å to ascertain the pore width at which the C_{hl} value observed for bulk water is recovered.

4. Conclusion

We have studied the influence of confinement on the hydration characteristics of confined NaCl solutions. Salt solutions at varying concentrations are confined between two graphitic surfaces separated by a distance, H. The hydration of ions is studied as a function of both the separation H and the salt concentration. Using a structural signature, we define the hydration limit as the salt concentration at which a sharp drop in the hydration number is observed. For bulk salt solutions, the hydration limit is expected to provide a lower bound on the solubility limit. At the hydration limit, a sharp change in all the ion–water PCFs is observed, indicating the lack of sufficient water to hydrate the ions. Although the hydration limit is expected to lie below the bulk solubility limit for the salt solution, it provides a suitable measure to compare the changes in hydration upon confinement. At low salt concentrations, a sharp decrease in hydration is observed for pore widths below $H = 10$ Å. At these small pores, confined water does not have bulk-like features and remains in a layered arrangement between the two surfaces. Despite this high degree of confinement, ions are able to form a quasi-2D hydration shell between the two surfaces. The hydration number reduces to about 4.15 at a pore width of $H = 8$ Å, when compared with the bulk hydration number of 6.25. At larger pore widths above $H = 16$ Å, where bulk-like water densities are observed in the central regions of the pore, the hydration number is above 6. Our study indicates the strong propensity of ions to form a hydration shell even under extremely severely confined aqueous environments. Furthermore, we observe that the hydration of ions only causes a weak perturbation to the oxygen density distributions between two surfaces. Upon comparing the hydration limits observed for bulk water with those obtained for confined aqueous solutions, a sharp drop in the hydration limit is observed for pore widths below $H = 10$ Å and the hydration limit reduces to about 55% of the bulk value at the smallest pore width of $H = 8$ Å. Although a large increase in the hydration limit occurs up to $H = 10$ Å, the bulk hydration limit is not recovered for the largest pore width of 20 Å examined in this study.

Acknowledgements

This work was carried out under a grant from the Department of Science and Technology, India and National Science Foundation (INT-0242921 and CBET-0730026/0314023).

References

[1] S. Murad, *Molecular dynamics simulations of osmosis and reverse osmosis in solutions*, Adsorption 2 (1996), pp. 95–101.
[2] J. Dzubiella, R.J. Allen, and J.P. Hansen, *Electric field-controlled water permeation coupled to ion transport through a nanopore*, J. Chem. Phys. 120 (2004), p. 5001.
[3] I. Vlassiouk, S. Smirnov, and Z. Siwy, *Ionic selectivity of single nanochannels*, Nano Lett. 8 (2008), p. 1978.
[4] Q. Shao, L. Huang, J. Zhou, L. Lu, L. Zhang, X. Lu, S. Jiang, K.E. Gubbins, and W. Shen, *Molecular simulation study of temperature effect on ionic hydration in carbon nanotubes*, Phys. Chem. Chem. Phys. 10 (2008), pp. 1896–1906.
[5] S. Koneshan, J.C. Rasaiah, R.M. Lynden-Bell, and S.H. Lee, *Solvent structure, dynamics, and ion mobility in aqueous solutions at 25°C*, J. Phys. Chem. B 102 (1998), pp. 4193–4204.
[6] A. Chandra, *Effects of ion atmosphere on hydrogen-bond dynamics in aqueous electrolyte solutions*, Phys. Rev. Lett. 85 (2000), pp. 768–771.

[7] S. Chowdhuri and A. Chandra, *Molecular dynamics simulations of aqueous NaCl and KCl solutions: Effects of ion concentration on the single-particle, pair, and collective dynamical properties of ions and water molecules*, J. Chem. Phys. 115 (2001), pp. 3732–3741.
[8] H.J. Bakker, *Structural dynamics of aqueous salt solutions*, Chem. Rev. 108 (2008), pp. 1456–1473.
[9] D. Nicholson and N. Quirke, *Ion pairing in confined electrolytes*, Mol. Sim. 29 (2003), pp. 287–290.
[10] H.T. Davis, H.S. White, and L. Zhang, *Simulations of solvent effects on confined electrolytes*, J. Chem. Phys. 98 (1993), pp. 5793–5799.
[11] Y.K.W. Tang, I. Szalai, and K.Y. Chan, *Diffusivity and conductivity of a primitive model electrolyte in a nanopore*, Mol. Phys. 99 (2001), pp. 309–314.
[12] A. Malani, K.G. Ayappa, and S. Murad, *Effect of confinement on the hydration and solubility of NaCl in water*, Chem. Phys. Lett. 431 (2006), pp. 88–93.
[13] R.M. Pashley and J.N. Israelachvili, *Molecular layering of water in thin films between mica surfaces and its relation to hydration forces*, J. Colloid Interface Sci. 101 (1984), pp. 511–523.
[14] E.S. Boek, P.V. Coveney, and N.T. Skipper, *Monte Carlo molecular modeling studies of hydrated Li-, Na- and K-smectites: Understanding the role of potassium as a clay swelling inhibitor*, J. Am. Chem. Soc. 117 (1995), pp. 12608–12617.
[15] D.A. Young and D.E. Smith, *Simulations of clay mineral swelling and hydration: Dependence upon interlayer ion size and charge*, J. Phys. Chem. B 104 (2000), pp. 9163–9170.
[16] A. Malani and K.G. Ayappa, *Adsorption isotherm of water on mica: Redistribution and film growth*, J. Phys. Chem. B 113 (2009), pp. 1058–1067.
[17] A. Malani, K.G. Ayappa, and S. Murad, *Influence of hydrophilic surface specificity on the structural properties of confined water*, J. Phys. Chem. B 113(42) (2009), pp. 13825–13839.
[18] H.J.C. Berendsen, J.R. Grigera, and T.P. Straatsma, *The missing term in effective pair potentials*, J. Phys. Chem. 91 (1987), pp. 6269–6271.
[19] J.C. Liu and P.A. Monson, *Does water condense in carbon pores?* Langmuir 12 (2005), pp. 10219–10225.
[20] R.H. Perry, D.W. Green, J.O. Maloney, *Perry's Chemical Engineers Handbook*, McGraw-Hill, New York, USA, 1997.
[21] S. Pal, G. Vishal, K.S. Gandhi, and K.G. Ayappa, *Ion exchange in reverse micelles*, Langmuir 21 (2005), pp. 767–778.
[22] T. Werder, J.H. Walther, R.L. Jaffe, T. Halicioglu, and P. Koumoutsakos, *On the water–carbon interaction for use in molecular dynamics simulations of graphite and carbon nanotubes*, J. Phys. Chem. B 107 (2003), pp. 1345–1352.
[23] H.C. Andersen, *Rattle: A "velocity" version of the shake algorithm for molecular dynamics calculations*, J. Compt. Phys. 52 (1983), pp. 24–34.
[24] M.P. Allen, D.J. Tildesley, *Computer Simulation of Liquids*, Oxford University Press, New York, USA, 1987.
[25] J.M. Haile, *Molecular Dynamics Simulation*, John Wiley & Sons, Inc., New York, USA, 1992.
[26] G.W. Neilson and J.E. Enderby, *Chapter 7. Neutron and X-ray diffraction studies of concentrated aqueous electrolyte solutions*, Annu. Rep. Prog. Chem., Sect. C: Phys. Chem. 76 (1979), pp. 185–220.
[27] S. Cummings, J.E. Enderby, G.W. Neilson, J.R. Newsome, R.A. Howe, W.S. Howells, and A.K. Soper, *Chloride ions in aqueous solutions*, Nature 287 (1980), pp. 714–716.
[28] J.R. Newsome, G.W. Neilson, and J.E. Enderby, *Lithium ions in aqueous solution*, J. Phys. C: Solid State Phys. 13 (1980), pp. L923–L926.
[29] J.E. Enderby and G.W. Neilson, *The structure of electrolyte solutions*, Rep. Prog. Phys. 44 (1981), pp. 593–653.
[30] J. Chandrasekhar, D.C. Spellmeyer, and W.L. Jorgensen, *Energy component analysis for dilute aqueous solutions of Li^+, Na^+, F^-, and $C1^-$ ions*, J. Am. Chem. Soc. 106 (1984), pp. 903–910.
[31] E. Sanz and C. Vega, *Solubility of KF and NaCl in water by molecular simulation*, J. Chem. Phys. 126 (2007), p. 014507.
[32] A. Striolo, A.A. Chialvo, P.T. Cummings, and K.E. Gubbins, *Water adsorption in carbon-slit nanopores*, Langmuir 19 (2003), pp. 8583–8591.